PHYSICAL REVIEW E **90**, 050702(R) (2014)

Path-integral calculation for the emergence of rapid evolution from demographic stochasticity

Hong-Yan Shih and Nigel Goldenfeld

Loomis Laboratory of Physics, Department of Physics, Center for the Physics of Living Cells and Institute for Genomic Biology, University of Illinois at Urbana-Champaign, 1110 West Green Street, Urbana, Illinois 61801-3080, USA

(Received 24 March 2014; published 26 November 2014)

Genetic variation in a population can sometimes arise so fast as to modify ecosystem dynamics. Such phenomena have been observed in natural predator-prey systems and characterized in the laboratory as showing unusual phase relationships in population dynamics, including a π phase shift between predator and prey (evolutionary cycles) and even undetectable prey oscillations compared to those of the predator (cryptic cycles). Here we present a generic individual-level stochastic model of interacting populations that includes a subpopulation of low nutritional value to the predator. Using a master equation formalism and by mapping to a coherent state path integral solved by a system-size expansion, we show that evolutionary and cryptic quasicycles can emerge generically from the combination of intrinsic demographic fluctuations and clonal mutations alone, without additional biological mechanisms.

DOI: 10.1103/PhysRevE.90.050702 PACS number(s): 87.23.−n, 87.18.Tt, 05.40.−a, 02.50.Ey

Predator-prey ecosystems exhibit noisy population oscillations whose origin is intuitively quite clear. The predator population number is activated by the prey and so increases. This in turn inhibits the growth of the prey population, but the decline of the prey leads to a corresponding decline in the predator number too. As a result, the prey population begins to rise and the cycle begins again. The simplicity of this narrative belies the difficulty of making a quantitative model of ecosystems. Strong demographic fluctuations degrade the utility of population-level modeling, rendering it problematic to assess the appropriate scales for ecological modeling [1–6] and even influencing community assembly on evolutionary time scales [7]. For example, observations of noisy periodicity in time series [8], slowly decaying correlations [9], and spatiotemporal patterns [10] clearly reflect the stochastic nature of populations [11,12] and their spatial organization. Moreover, even the simplest predator-prey systems exhibit complex spatial structure. This can arise through a variety of pattern formation processes [13–17] that include recent results on deterministic [18,19] and fluctuation-induced Turing instabilities [10,20,21], traveling waves [17,22,23], and even analogies to the processes of phase separation in binary alloys [24]. In short, collective and stochastic many-body phenomena are ubiquitous in biology and perhaps nowhere more so than in ecology.

The classical literature on predator-prey systems [25] assumes that evolution occurs on such long time scales that it can be neglected, but it is not obvious that this is always valid [26]. Recent work using rotifers (predator) and algae (prey) in a chemostat shows that dramatic changes in the population structure of the rotifer-algae predator-prey system can arise from rapid responses to intense selection among induced genetically distinct strains [27–34]. In these studies, so-called sub-populations with different traits emerge from evolution and lead to new trophic structures, accompanied by anomalous ecological dynamics. These anomalies include evolutionary cycles with long oscillation periods in population dynamics and predator-prey phase shifts near π (and definitely distinct from the canonical value of $\pi/2$), and cryptic cycles, in which prey populations remain almost constant while the predator population oscillates. Such phenomena have been modeled with deterministic differential equations containing empirical descriptions of functional response with a variety of detailed hypotheses on the mechanism of species interactions for rapid evolution [28–30,33,35–39] or nonheritable phenotypic plasticity [40]. Such models are not only very complex, with many adjustable parameters, but also cannot capture the stochasticity evident in the observations.

The purpose of this Rapid Communication is to propose and analyze a minimal model for rapid evolution that includes the effects of demographic stochasticity. Using tools from statistical mechanics, demographic stochasticity has been successfully captured using individual-level models (ILMs) in a variety of situations that range from simple well-mixed predator-prey interactions [41–43] to spatially extended systems that can exhibit quasi-Turing patterns [20,21,23,44–46]. Here we propose an ILM for rapid evolution that we solve analytically by mapping the model into a coherent-state path-integral representation [47–51] (for a review and history, see Ref. [52]) followed by a volume expansion [53] to derive the effective Langevin equation for demographic fluctuations. Accompanied by Gillespie simulation [54] for the model, we show that this simple stochastic model can predict rapid evolution phenomena in well-mixed systems, yielding phase diagrams that are similar to those of more complex deterministic models and in qualitative agreement with available data. Thus key aspects of rapid evolution can be minimally modeled by subpopulation dynamics driven simply by intrinsic demographic stochasticity, without additional biological mechanisms. Our model can serve as a starting point for analyzing spatial distributions and large fluctuations such as extinction.

The physical explanation for anomalous cycles was understood early on [28]. In contrast to the $\pi/2$ phase shift of the conventional predator-prey model, evolutionary cycles with a π phase shift can arise because of the existence of a mutant prey population that can defend itself from the predator but which incurs a metabolic cost. The defended prey compete with the wild type for nutrients and thus delay the regrowth of the wild-type prey. The resulting additional phase lag of the wild-type prey behind the defended prey is about $\pi/2$ because the wild-type prey must grow back before the population of the defended prey will return to its minimum level. When the defended prey have very effective defense without significant

metabolic cost, there is substantial delay of the regrowth of the wild-type prey. If the wild-type prey lag the defended prey by π, their fluctuations offset each other and thus the dynamics of the total prey population appears in aggregate to be suppressed, leading to the cryptic cycles.

An ILM for rapid evolution. To model this quantitatively, consider a model for a system composed of nutrients for the prey N, the vulnerable (wild-type) prey W, the so-called defended (mutant) prey D, and the predator P. The basic individual processes for them are regrowth of nutrients, reproduction of prey, predation by predator, death, and migration to the nearest site for all individuals:

$$\begin{aligned} &\emptyset_i \xrightarrow{b} N_i, \quad N_i R_i \xrightarrow{\frac{c_R}{V}} R_i R_i, \quad R_i P_i \xrightarrow{\frac{p_R}{V}} P_i P_i, \\ &S_i \xrightarrow{d_S} \emptyset_i, \quad S_i \xrightarrow[\langle ij\rangle]{\nu_S} S_j, \end{aligned} \tag{1}$$

where $\emptyset_i$ denotes the empty state at site i, $R = W,D$ is the prey index, S_i represents species $S = N,W,D,P$ at site i, and V is an effective coarse-grained or correlation volume in which there is no significant population spatial variation. In ecology, V is called the patch size and it acts as a control on the amplitude of demographic fluctuations. Because V is larger than the mean volume per organism, we will make analytical progress by using an expansion in inverse powers of V. The defended prey experiences a smaller predation rate than the wild-type prey, i.e., $p_D < p_W$, and also has a smaller reproduction rate or larger degeneration rate due to the metabolic cost for defense, i.e., $c_W > c_D$ or $d_W < d_D$. For the nutrients, ν_N and d_N are set to zero. The corresponding master equation that defines the time evolution of the probability distribution of population states is

$$\begin{aligned} &\partial_t P\big(\{n_{S_i}\}\big) \\ &= \sum_{\{n_{S_i}\}} \Bigg\{ b\big(E_{N_i}^{-1} - 1\big)\big(n_{N_i}^{\max} - n_{N_i}\big) + \sum_S d_S\big(E_{S_i} - 1\big)n_{S_i} \\ &\quad + \sum_R \left[\frac{c_R}{V}\big(E_{N_i}E_{R_i}^{-1} - 1\big)n_{N_i}n_{R_i} \right. \\ &\quad \left. + \frac{p_R}{V}\big(E_{R_i}E_{P_i}^{-1} - 1\big)n_{R_i}n_{P_i} \right] \Bigg\} P\big(\{n_{S_i}\}\big), \end{aligned} \tag{2}$$

where $\{\cdots\}$ denotes the set over all sites and species, the prey index $R = W,D$, and the step operators $E_{S_i}^{\pm}$ are defined as $E_{S_i}^{\pm} f(\{n_{S_i}\}) = f(\{n_{S_i} \pm 1\})$.

Spatial extension. To complete the specification of the model, we need to include particle diffusion, for which the Doi formalism [47] is especially convenient. The resulting spatially extended model represents a nonperturbative formulation of the model and can be used to study spatial patterns and large demographic fluctuations that are important near the ecosystem extinction transition, where the predator population vanishes [23,55]. The procedure is to write Eq. (2) as a second-quantized Hamiltonian and then express the generating functional for probabilities and correlations as a path integral [48,49,51,52].

Following the standard procedure, we introduce the probability state vector in the Fock space constructed by different occupation number states

$$|\psi\rangle = \sum_{\{n_{S_i}\}} P\big(\{n_{S_i}\}\big)\big|\{n_{S_i}\}\big\rangle \tag{3}$$

so that the master equation becomes a Liouville equation

$$\partial_t|\psi\rangle = -\hat{H}|\psi\rangle, \tag{4}$$

with the Liouvillian $\hat{H} = \sum_i \hat{H}_i$,

$$\begin{aligned} \hat{H}_i &= b\big(1 - \hat{a}_{N_i}^{\dagger}\big)\big(n_{N_i}^{\max} - \hat{a}_{N_i}^{\dagger}\hat{a}_{N_i}\big) \\ &\quad + \sum_R \left[\frac{c_R}{V}\big(\hat{a}_{N_i}^{\dagger}\hat{a}_{N_i}\hat{a}_R^{\dagger}\hat{a}_{R_i} - \hat{a}_{N_i}\hat{a}_{R_i}^{\dagger 2}\hat{a}_{R_i}\big) \right. \\ &\quad \left. + \frac{p_R}{V}\big(\hat{a}_{R_i}^{\dagger}\hat{a}_{R_i}\hat{a}_{P_i}^{\dagger}\hat{a}_{P_i} - \hat{a}_{R_i}\hat{a}_{P_i}^{\dagger 2}\hat{a}_{P_i}\big) \right] \\ &\quad + \sum_S \left[d_S\big(\hat{a}_{S_i}^{\dagger}\hat{a}_{S_i} - \hat{a}_{S_i}\big) + \nu_S \sum_{j\in N.N.} \big(\hat{a}_{S_i}^{\dagger} - \hat{a}_{S_j}^{\dagger}\big)\hat{a}_{S_i} \right], \end{aligned} \tag{5}$$

where $\hat{a}_{S_i}^{\dagger}$ and $\hat{a}_{S_i}$ are bosonic raising and lowering number operators for species S at site i. Equations (4) and (5) are exact and naturally allow the representation of the many-body path-integral formalism. Using the standard mapping to the coherent-state path-integral representation and applying the volume expansion method, the effective Lagrangian density for Gaussian-order fluctuations becomes

$$\mathcal{L}^{(2)} = \tilde{\boldsymbol{\rho}}^T\partial_t\boldsymbol{\xi} - \tilde{\boldsymbol{\rho}}^T\mathbf{A}[\{\phi_S\}]\boldsymbol{\xi} - \tfrac{1}{2}\tilde{\boldsymbol{\rho}}^T\mathbf{B}[\{\phi_S\}]\boldsymbol{\xi}, \tag{6}$$

where $\boldsymbol{\xi} = (\xi_N,\xi_W,\xi_D,\xi_P)$ and $\tilde{\boldsymbol{\rho}} = (\tilde{\rho}_N,\tilde{\rho}_W,\tilde{\rho}_D,\tilde{\rho}_P)$ are the fluctuation field vectors and $\mathbf{A}$ and $\mathbf{B}$ are functions of the mean-field densities $\{\phi_S\}$ given in Ref. [56]. Equation (6) is equivalent to the Langevin equations as a function of wave number k and time:

$$\begin{aligned} &\frac{d\boldsymbol{\xi}}{dt} = \mathbf{A}\boldsymbol{\xi} + \boldsymbol{\gamma}, \\ &\langle\gamma_S(k,t)\gamma_{S'}(k',t')\rangle = \mathbf{B}_{SS'}(2\pi)^d\delta(k-k')\delta(t-t'). \end{aligned} \tag{7}$$

In contrast to deterministic models [27–38,40], the dynamics depends not only on the Jacobian $\mathbf{A}[\{\phi_S\}]$ from the mean-field equation but also on the covariance matrix $\mathbf{B}[\{\phi_S\}]$. Since $\mathbf{B}_{RR'}[\{\phi_S\}]$ in Eq. (7) is governed by the macroscopic densities, the white noise $\boldsymbol{\gamma}$ that determines the dynamics of fluctuations is effectively multiplicative. Without the white noise $\boldsymbol{\gamma}$, the solutions for $\boldsymbol{\xi}$ in the Langevin equations in Eq. (7) contributed by the linear terms are expected to decay exponentially and converge to mean-field densities $\{\phi_S\}$. However, the multiplicative white noise plays an important role: Whenever it can cancel out the contribution of the eigenvalues of $\mathbf{A}$, $\boldsymbol{\xi}$ will be persistently driven away from convergent mean-field densities, i.e., white noise can select the frequency in the deterministic equations, resulting in periodic and strongly fluctuating population dynamics and spatial patterns. This is a resonant effect induced by demographic stochasticity through shot noise [41] with the resonant frequency near the slowest decaying mode in the mean-field solutions. Since the systems in the rotifer-algae experiments are well mixed, the diffusion terms are neglected in the following calculation and simulation.

Power spectrum, phase relationship, and phase diagram. The power spectrum of demographic noise has a resonant frequency corresponding to the deterministic eigenvalue. The power spectrum of species S, $P_{SS}(\omega)$, can be calculated by taking the Fourier transform of the Langevin equations (7),

$$P_{SS'}(\omega) = \langle \tilde{\xi}_S(\omega)\tilde{\xi}_{S'}(-\omega)\rangle, \tag{8}$$

and setting $S' = S$. The Fourier transform gives the autocorrelation function, which has the form of a polynomial of degree 6 divided by a polynomial of degree 8, yielding a power-law tail proportional to ω^{-2} at large ω, as expected for quasicycles in other systems [20,42]. The power spectrum $P_{SS}(\omega)$ peaks at a resonant frequency that is smaller than the oscillation frequency of the deterministic solution because of the renormalization by the white noise in Eq. (7) [46]. The longer period reflects the presence of the defended prey that causes the delay of the regrowth of the wild-type prey and the predator. The phase difference between the fluctuation fields is defined as

$$\theta_{SS'}(\omega) = \tan^{-1}\frac{\mathrm{Im}[P_{SS'}(\omega)]}{\mathrm{Re}[P_{SS'}(\omega)]}. \tag{9}$$

The phase difference between total prey and the predator $\theta_{(W+D)P}$ can be calculated from $P_{(W+D)P}(\omega) = \langle(\tilde{\xi}_W(\omega) + \tilde{\xi}_D(\omega))\tilde{\xi}_P(-\omega)\rangle = P_{WP}(\omega) + P_{DP}(\omega)$.

The results of analytic calculations and simulations based on Eq. (1) are shown in Fig. 1. We use the Gillespie algorithm [54] for stochastic simulations and introduce random mutation from the wild-type prey to the defended prey. The mutation is added purely to seed a new subpopulation to see the dramatic impact of the fixed subpopulation after mutations, but plays no significant role in the subsequent dynamics; thus mutations are neglected in our analytical calculations below. The subsequent anomalous dynamics due to the presence of this subpopulation is conventionally called evolution in the ecological literature, because the presence of the additional strain emerges from mutation, and we are interested in following the frequency in the population of the mutant strain. We tried to simulate the experimental results of the rotifer-algae chemostat, where the control parameters are the nutrient concentration in flow media $\phi_N^{\max}$ and the dilution rate b. The natural degradation rates of the wild-type prey and predator are assumed to be much slower than the dilution rate and therefore $b \approx d_P \approx d_W < d_D$ (the defended prey is less healthy). In Fig. 1(a), at first there are only the wild-type prey and the predator in the system and the dynamics exhibits normal cycles where the predator lags behind the prey by $\pi/2$. When predation pressure is high, around $t \sim 400$, a mutation has given rise to a defended prey population that subsequently adapts to dominate the population and causes additional delay in growth of the wild-type prey and the predator, leading to evolutionary cycles with a π phase shift between the total prey and the predator. Figure 1(b) shows an example of cryptic cycles, where the defended prey has a similar reproduction rate as that of the wild-type prey, i.e., $c_D \sim c_W$, and the defended prey can advance the wild-type prey by nearly π and thus the total prey population is suppressed. The quasicycle calculations in Figs. 1(f)–1(h) for the power spectrum and the phase spectrum well predict the simulation results in Figs. 1(c)–1(e). Besides the expected randomness in the dynamics from the stochastic

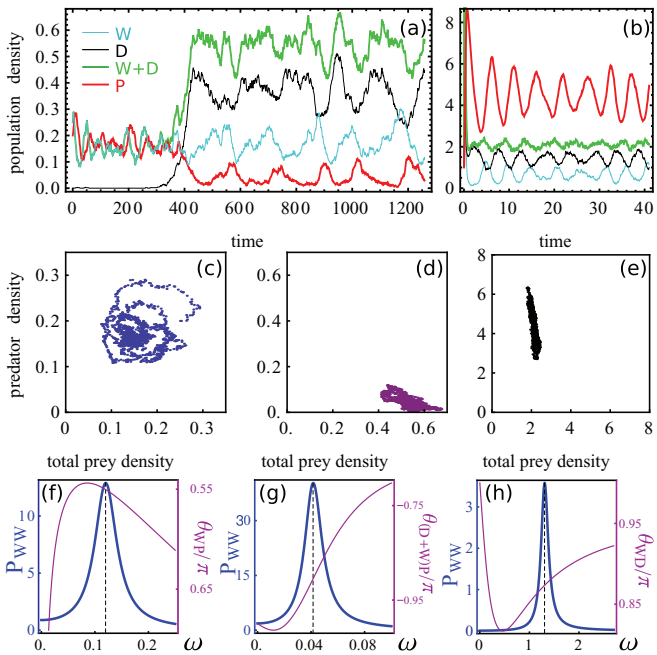

FIG. 1. (Color online) Stochastic simulations for (a) evolutionary cycles emerging from normal cycles due to random mutation and (b) cryptic cycles. Phase portraits of the steady states of (c) normal cycles and (d) evolutionary cycles from the stochastic simulations show that the phase differences between predator and the total prey population are roughly $\pi/2$ and π, respectively, while for (e) cryptic cycles there is no obvious phase relationship. (f)–(h) Power spectrum of the wild-type prey (thick curve) and phase difference spectrum (thin curve) from analytic calculations based on ILMs. The estimated phase differences are -0.55π and 0.905π for (f) normal cycles and (g) evolutionary cycles and for (h) cryptic cycles the predicted phase difference between the wild-type prey and the defended prey is approximately 0.874π. The parameter values are (a) $V = 1000$, $c_W = 0.3$, $p_W = 0.6$, $c_D/c_W = 0.8$, $p_D/p_W = 0.01$, $d_D/d_W = 1$, $\phi_{N,\max} = 1$, and $b = 0.1$ and (b) $V = 380$, $c_W = 60$, $p_W = 0.92$, $c_D/c_W = 0.95$, $p_D/p_W = 0.001$, $d_D/d_W = 7.5$, $\phi_{N,\max} = 16$, and $b = 0.1$.

simulation, Figs. 1(a) and 1(b) also show similar asymmetric profiles and the longer period after the subpopulation emerges, as in the experimental data in [27–32,34].

The phase diagram is usually studied by linear stability analysis of the mean-field equations [see, for example, Eqs. (7)–(9) in Ref. [56]]. To reduce the dimension of parameter space, variables are rescaled to be dimensionless: $\bar{t} \equiv bt$, $\bar{d}_S \equiv d_S/b$, $\bar{\phi}_S \equiv /\phi_N^{\max}$, $\bar{c}_S \equiv c_S\phi_N^{\max}/b$, and $\bar{p}_S \equiv p_S\phi_N^{\max}/b$. However, this rescaling is rather subtle in stochastic calculations. For example, matrices **A** and **B** from Eq. (7) scale with $1/\phi_N^{\max}$ as mean fields ϕ_S, but γ in Eq. (7) rescales with $1/\sqrt{\phi_N^{\max}}$, resulting in

$$\frac{\xi_S}{\phi_S} \sim \frac{1}{\sqrt{\phi_N^{\max}}}\frac{\bar{\xi}_S}{\bar{\phi}_S}, \tag{10}$$

where $\bar{\xi}_S$ are the rescaled demographic noise fields. Therefore, for two stochastic individual-level models with the same mean-field limit after rescaling, demographic fluctuations are more important in the model with smaller nutrient carrying capacity $V\phi_N^{\max}$. Thus neglecting fluctuations as in the

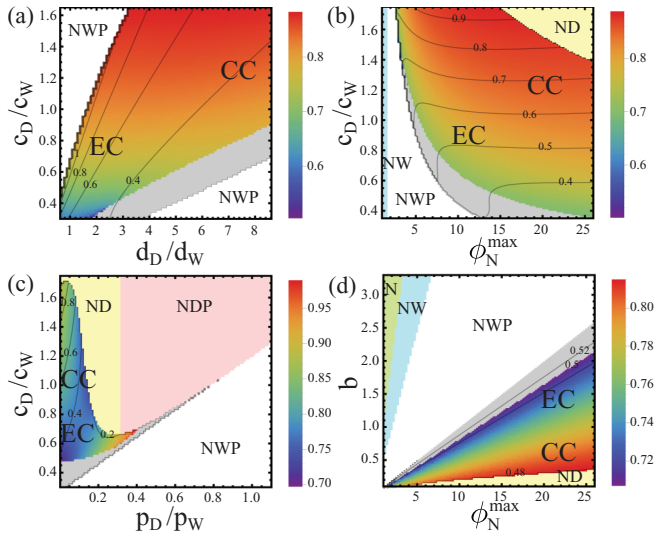

FIG. 2. (Color online) Phase diagrams for evolutionary cycles (EC) and cryptic cycles (CC) calculated from ILMs with respect to the ratio of the prey reproduction rate c_D/c_W, the ratio of the predation rate p_D/p_W, the maximum nutrient concentration $\phi_N^{\max}$, and the dilution rate b. The gradient-colorful region corresponds to the coexistence of all species and in the other regions the rapid evolution is not stable, with corresponding letters indicating the coexistence of only certain species. The coexistence states are decided by the mean-field densities and their ratio to the fluctuations; when fluctuations are larger than mean-field solutions, the dynamics is under high risk of extinction. The color legend represents the predicted phase difference between the wild-type prey and the defended prey θ_{WD} for rapid evolution, in units of π. The contours are the estimated amplitude ratios of wild-type prey to predator, indicating the tendency to be cryptic cycles. In the gray region near transition, the two types of prey start to decouple, leading to degenerate peaks in power spectra, and thus the phase is not well defined. Except for the axis specified in each diagram, the parameters in the calculations are $V = 300$, $c_W = 1$, $p_W = 1$, $c_D/c_W = 0.8$, $p_D/p_W = 0.01$, $d_D/d_W = 3.5$, $\phi_N^{\max} = 16$, and $b = 0.6$. The predicted phase diagram is consistent with stochastic simulation.

conventional rescaling for mean-field equations can potentially cause unphysical predictions for the phase diagram. To avoid this situation, we examine the stability of solutions by comparing the amplitude of the lowest-order population fluctuations with their mean fields.

Figure 2 shows the calculated phase diagrams of ILMs in Eq. (1). In Fig. 2(a), due to the cost for defense, the defended prey have an inferior reproduction rate ($c_D < c_W$) or are unhealthier than the wild-type prey ($d_D > d_W$), leading to evolutionary cycles. When the cost of reproduction is low, cryptic cycles can occur, where $\theta_{WD} \approx \pi$. If c_D is moderate, it is possible to have a correspondingly high death rate and thus the fluctuations of prey are suppressed relative to the wild-type prey, causing the dynamics to be cryptic. In Fig. 2(b), under high $\phi_N^{\max}$, the defended prey are more likely to grow and dominate the system, which causes the wild-type prey to experience a greater phase lag than the defended prey, and the dynamics tends towards a completely cryptic cycle. In Fig. 2(c), if p_D is low, then higher c_D can lead to more phase delay and thus gives cryptic cycles. When p_D increases, the predator has greater food resources available from the defended prey, yielding a larger population, which then consumes more of the wild-type prey; this in turn reduces the wild-type prey population and leads to the dominance of the defended prey. In such a situation, the wild-type prey experiences a greater phase delay (nearly π) behind the defended prey, but the wild-type prey population is too small to cancel out the fluctuations of the defended prey population and thus the dynamics cannot be characterized as cryptic. Our result in Fig. 2(c) predicts a phase diagram that is similar to but slightly different from that of Fig. 3 in [29]; the region where all species coexist as predicted by the stochastic model is smaller than the deterministic solutions because of extinction fluctuations near phase boundaries. In Fig. 2(d), under small b, i.e., slow supplement of the nutrient and low reduction rate from dilution, although both subpopulations of the prey have low reproduction, the wild-type prey population decreases more due to predation while the defended prey has a greater chance to compete for nutrients; thus the system is more likely to show cryptic cycles.

Our results show that rapid evolution strongly renormalizes the ecosystem time scale and the prediction of the coexistence region can help estimate the risk of extinction and the impact of the rate of environmental changes (for example, the dilution rate and nutrient concentration in the rotifer-algae system). Our model can also be used to study spatial-extended situations in natural ecosystems or laboratory experiments that are not in a well-mixed chemostat.

In summary, we have shown clearly that a generic stochastic individual-level model can yield rapid evolution phenomena and that anomalous dynamics can arise without special assumptions or fine-tuning, in sharp contrast to existing results in the ecology literature based on deterministic models. We expect this description to be especially useful to study the transition to rapid evolution from normal cycles since before the transition the mutant prey population has low relative abundance and is thus likely to exhibit strong effects of demographic stochasticity and spatiotemporal fluctuations.

We thank S.P. Ellner and U. Täuber for helpful discussions. This material is partially supported by the National Aeronautics and Space Administration through the NASA Astrobiology Institute under Cooperative Agreement No. NNA13AA91A issued through the Science Mission Directorate.

[1] S. A. Levin, Ecology **73**, 1943 (1992).

[2] J. Bascompte and R. V. Solé, Trends Ecol. Evol. **10**, 361 (1995).

[3] M. Pascual and S. A. Levin, Ecology **80**, 2225 (1999).

[4] M. Pascual, P. Mazzega, and S. A. Levin, Ecology **82**, 2357 (2001).

[5] N. Goldenfeld and C. Woese, Annu. Rev. Condens. Matter Phys. **2**, 375 (2011).

[6] J. Chave, Ecol. Lett. **16**, 4 (2013).
[7] Y. Murase, T. Shimada, N. Ito, and P. A. Rikvold, Phys. Rev. E **81**, 041908 (2010).
[8] C. Elton and M. Nicholson, J. Anim. Ecol. **11**, 215 (1942).
[9] M. Pineda-Krch, H. J. Blok, U. Dieckmann, and M. Doebeli, Oikos **116**, 53 (2007).
[10] J. A. Bonachela, M. A. Muñoz, and S. A. Levin, J. Stat. Phys. **148**, 724 (2012).
[11] M. B. Bonsall and A. Hastings, J. Anim. Ecol. **73**, 1043 (2004).
[12] D. L. DeAngelis and W. M. Mooij, Annu. Rev. Ecol. Evol. Syst. **36**, 147 (2005).
[13] E. Meron, Ecol. Model. **234**, 70 (2012).
[14] A. Liebhold, W. D. Koenig, and O. N. Bjørnstad, Annu. Rev. Ecol. Evol. Syst. **35**, 467 (2004).
[15] H. Malchow, F. M. Hilker, I. Siekmann, S. V. Petrovskii, and A. B. Medvinsky, *Aspects of Mathematical Modelling* (Springer, Berlin, 2008), pp. 1–26.
[16] R. HilleRisLambers, M. Rietkerk, F. van den Bosch, H. H. Prins, and H. de Kroon, Ecology **82**, 50 (2001).
[17] B. Blasius, A. Huppert, and L. Stone, Nature (London) **399**, 354 (1999).
[18] S. Levin and L. Segel, Nature (London) **259**, 659 (1976).
[19] S. Kinast, Y. R. Zelnik, G. Bel, and E. Meron, Phys. Rev. Lett. **112**, 078701 (2014).
[20] T. Butler and N. Goldenfeld, Phys. Rev. E **80**, 030902(R) (2009).
[21] T. Butler and N. Goldenfeld, Phys. Rev. E **84**, 011112 (2011).
[22] J. A. Sherratt, M. A. Lewis, and A. C. Fowler, Proc. Natl. Acad. Sci. U.S.A. **92**, 2524 (1995).
[23] M. Mobilia, I. T. Georgiev, and U. C. Täuber, J. Stat. Phys. **128**, 447 (2007).
[24] Q.-X. Liu, A. Doelman, V. Rottschfer, M. de Jager, P. M. J. Herman, M. Rietkerk, and J. van de Koppel, Proc. Natl. Acad. Sci. U.S.A. **110**, 11905 (2013).
[25] A. A. Berryman, Ecology **73**, 1530 (1992).
[26] J. N. Thompson, Trends Ecol. Evol. **13**, 329 (1998).
[27] G. F. Fussmann, S. P. Ellner, K. W. Shertzer, and N. G. Hairston, Jr., Science **290**, 1358 (2000).
[28] T. Yoshida, L. E. Jones, S. P. Ellner, G. F. Fussmann, and N. G. Hairston, Nature (London) **424**, 303 (2003).
[29] T. Yoshida, S. P. Ellner, L. E. Jones, B. J. M. Bohannan, R. E. Lenski, and N. G. Hairston, Jr., PLoS Biol. **5**, e235 (2007).
[30] L. Jones and S. Ellner, J. Math. Biol. **55**, 541 (2007).
[31] L. Becks, S. P. Ellner, L. E. Jones, and N. G. Hairston, Jr., Ecol. Lett. **13**, 989 (2010).
[32] L. Becks, S. P. Ellner, L. E. Jones, and N. G. Hairston, Jr., Ecol. Lett. **15**, 492 (2012).
[33] B. J. M. Bohannan and R. E. Lenski, Ecology **78**, 2303 (1997).
[34] S. P. Ellner, Funct. Ecol. **27**, 1087 (2013).
[35] K. W. Shertzer, S. P. Ellner, G. F. Fussmann, and N. G. Hairston, J. Anim. Ecol. **71**, 802 (2002).
[36] A. Yamauchi and N. Yamamura, Ecology **86**, 2513 (2005).
[37] M. H. Cortez and S. P. Ellner, Am. Nat. **176**, E109 (2010).
[38] A. Mougi, Theor. Popul. Biol. **81**, 113 (2012).
[39] A. Mougi, J. Theor. Biol. **305**, 96 (2012).
[40] M. Yamamichi, T. Yoshida, and A. Sasaki, Am. Nat. **178**, 287 (2011).
[41] A. J. McKane and T. J. Newman, Phys. Rev. Lett. **94**, 218102 (2005).
[42] S. Morita, Y. Itoh, and K.-I. Tainaka, J. Phys. Soc. Jpn. **74**, 819 (2005).
[43] A. J. Black and A. J. McKane, Trends Ecol. Evol. **27**, 337 (2012).
[44] C. A. Lugo and A. J. McKane, Phys. Rev. E **78**, 051911 (2008).
[45] T. Butler and D. Reynolds, Phys. Rev. E **79**, 032901 (2009).
[46] U. C. Täuber, J. Phys. A: Math. Theor. **45**, 405002 (2012).
[47] M. Doi, J. Phys. A: Math. Gen. **9**, 1465 (1976).
[48] P. Grassberger and M. Scheunert, Fortschr. Phys. **28**, 547 (1980).
[49] A. Mikhailov, Phys. Lett. A **85**, 214 (1981).
[50] N. Goldenfeld, J. Phys. A: Math. Gen. **17**, 2807 (1984).
[51] L. Peliti, J. Phys. (Paris) **46**, 1469 (1985).
[52] D. C. Mattis and M. L. Glasser, Rev. Mod. Phys. **70**, 979 (1998).
[53] N. van Kampen, Can. J. Phys. **39**, 551 (1961).
[54] D. T. Gillespie, J. Phys. Chem. **81**, 2340 (1977).
[55] M. Parker and A. Kamenev, J. Stat. Phys. **141**, 201 (2010).
[56] See Supplemental Material at http://link.aps.org/supplemental/10.1103/PhysRevE.90.050702 for a detailed derivation.